Adaptive double-integral-sliding-mode-maximum-power-point tracker for a photovoltaic system

Bidyadhar Subudhi[1], *Raseswari Pradhan*[2]

[1]*Department of Electrical Engineering, Centre of Excellence for Renewable Energy & Control, National Institute of Technology Rourkela, Rourkela 769 008, Orissa, India*
[2]*School of Electrical Engineering, Veer Surendra Sai University of Technology, Sambalpur-768018*
E-mail: bidyadhar@nitrkl.ac.in

Published in *The Journal of Engineering*; Received on 14th July 2015; Accepted on 28th August 2015

Abstract: This study proposed an adaptive double-integral-sliding-mode-controller-maximum-power-point tracker (DISMC-MPPT) for maximum-power-point (MPP) tracking of a photovoltaic (PV) system. The objective of this study is to design a DISMC-MPPT with a new adaptive double-integral-sliding surface in order that MPP tracking is achieved with reduced chattering and steady-state error in the output voltage or current. The proposed adaptive DISMC-MPPT possesses a very simple and efficient PWM-based control structure that keeps switching frequency constant. The controller is designed considering the reaching and stability conditions to provide robustness and stability. The performance of the proposed adaptive DISMC-MPPT is verified through both MATLAB/Simulink simulation and experiment using a 0.2 kW prototype PV system. From the obtained results, it is found out that this DISMC-MPPT is found to be more efficient compared with that of Tan's and Jiao's DISMC-MPPTs.

1 Introduction

Photovoltaic (PV) systems have low energy conversion efficiency due to their non-linear and time-varying I–V and P–V characteristics with respect to variation in solar irradiance and PV cell temperature. Hence, the PV systems need to be operated at their maximum-power-point (MPPs). To track the MPP, a maximum-power-point tracker (MPPT) is usually placed between a PV panel and load. MPP tracking is an important aspect in a PV system because at MPP, a PV panel operates most efficiently as it delivers the maximum power.

The literature of MPPT is very broad and a number of MPPT techniques have been proposed and implemented [1]. A comprehensive comparative analysis of some of the popular and latest MPPT techniques has been made in [2]. Perturb and observe (P&O) is the most popular technique because of its accuracy and ease in practical implementation [3, 4]. In this technique, the input PV voltage is perturbed in small step sizes to determine the direction of the MPP and moves the operating point of the PV system accordingly. Although this approach is simple to implement and a priori knowledge of the PV system is not required, but calculated MPP in this MPPT technique oscillates around the actual MPP depending on the perturbation size even under constant environmental conditions [5]. An alternative method known as incremental conductance (Inc-Cond) has been designed to resolve this issue to some extent by nullifying sum of the slope of PV power and the dynamic resistance of the PV array at the MPP [6]. As a result, this algorithm estimates the slope of the power curve by incrementing the PV voltage until this estimated sum oscillates about zero. In this case, calculated MPP still oscillates around real MPP which leads to PV voltage oscillations and inefficiency in fast changing weather conditions. Recently, some adaptive P&O and adaptive Inc-Cond techniques have been developed which exhibit improved tracking responses than that of P&O [7–9]. However, P&O and Inc-Cond-based techniques have a drawback of yielding limit cycles. Ideally, one desires a peak seeking scheme that is asymptotically convergent and self-optimising with respect to shifts in the MPP [10].

The above discussion motivates for designing a robust sliding-mode control MPPT (SMC-MPPT) as SMC possesses inherent robustness and stability. In SMC-MPPT, tracking error is considering as sliding surface [11]. Furthermore, it has high degree of flexibility in design choices and also easy to implement using inexpensive digital signal processing, microcontroller and field programmable gate array (FPGA) etc. However, to handle rapid variations of environmental conditions for a wide range, this SMC-MPPT would require large inductances and capacitances in its MPPT converter. By using SMC with pulse width modulation (PWM) concept, size of these inductances and capacitances can be reduced. However, SMC with PWM has a major drawback, that is, presence of high-frequency chattering, unwanted tracking error, slow response and large tracking time [12]. In some of the recent works, improvement has been made in the SMC-MPPT so that it is now enriched with fast convergence, simplicity and self-optimisation [13–18]. However, the problem of fluctuations in PV voltage due to high-frequency chattering and tracking error are still present in the PV system. To tackle these problems, a new SMC-based controller called integral-sliding-mode controller (ISMC) has been designed [19] in which an integral term of tracking error has been added to the existing sliding surface of SMC. To further improve the tracking performance, another integral term of tracking error is added to the existing sliding surface of ISMC and it is called as a double-ISMC (DISMC) [20]. A DISMC has fast dynamic responses for a wide range of operating conditions. It also inherits the robustness and stability features of SMC.

Like SMC, selection of sliding surface is very important in designing a DISMC because the controller design and efficiency are directly dependent on the sliding surface. There are some DISMCs available in the literatures [20–22] in voltage regulation of DC/DC converter applications such as Tan's DISMC [20] and Jiao's DISMC [22]. MPPT with DISMC concept is first introduced in [21]. In this paper, a DISMC-MPPT has been designed with a new sliding surface and its tracking performance is found to be better than that of DISMC-MPPT with Jiao's sliding surface and Tan's sliding surface. However, one distinct shortcoming of this DISMC-MPPT is that here a fixed sliding surface is used and the sliding surface parameters have empirically chosen fixed values. This particular drawback restricts performance range of the DISMC-MPPT [22]. To avoid this situation, a new adaptive DISMC-MPPT is designed in this paper whose sliding surface parameters are tuned with the reference MPP voltage. Therefore, this proposed adaptive DISMC-MPPT is providing better tracking responses than that of DISMC-MPPT [23] in terms of tracking time and voltage oscillation at steady state. Efficacy of this new

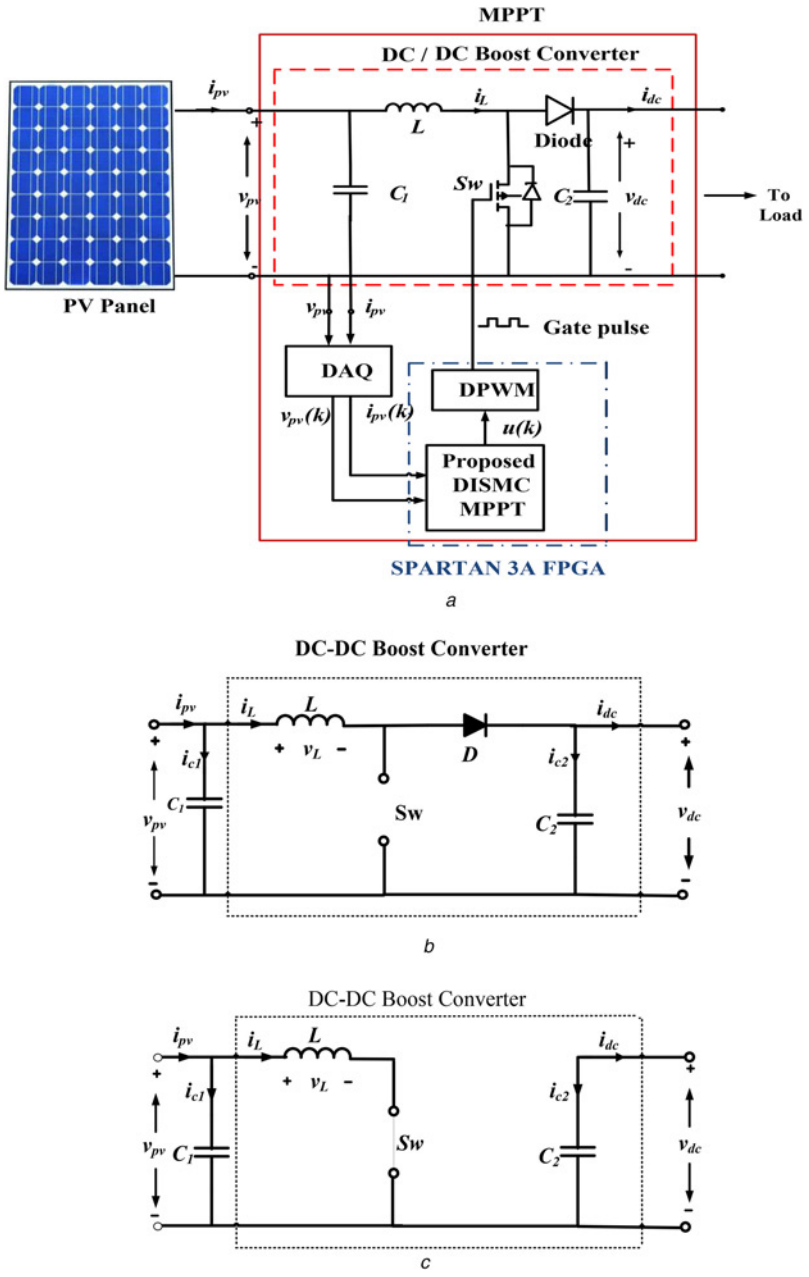

Fig. 1 *Problem formulation*
a Block diagram of a simple PV system topology with DISMC-based MPPT, equivalent circuit of boost converter
b When Sw is open ($u = 0$)
c Circuit when Sw is closed ($u = 1$)

adaptive DISMC-MPPT has been verified with simulation and experimental results using a 0.2 kW prototype PV system.

The major contributions of this paper are as follows:

i. Design of a new variable step MPPT algorithm to estimate MPP voltage.

ii. Design of a DISMC controller with a new sliding surface where the controller parameters have been tuned ensuring the reaching and stability conditions of the sliding surface, and achieving guaranteed stability of the proposed MPPT controller.

iii. The proposed MPPT has ease in implementation and understanding.

iv. The proposed DISMC-MPPT control algorithm has been validated using simulation and experimental studies.

Rest of this paper is organised as follows. The MPPT problem for a PV system is formulated in Section 2. In Section 3, the proposed DISMC is derived. Simulation results and experimental results for control implementation are discussed in Section 4. Section 5 further displays the concluding remarks.

2 Problem formulation

Fig. 1*a* describes a topology of a stand-alone PV system. It consists of a PV panel, a DC/DC boost converter and a load and a control circuit that generates PWM signal to the boost converter for MPPT operation. It also has two filters one between boost converter and inverter and another between inverter and load to damp out the ripple in the DC-link voltage v_{dc}, DC-link current i_{dc}, output voltage v_{ac} and output current i_{ac}. The PV output current i_{pv} can be expressed as [24]

$$i_{pv} = I_{pv} - I_0\left[\exp\left(\frac{v_{pv} + i_{pv}R_s}{N_s V_t}\right) - 1\right] - \frac{v_{pv} + i_{pv}R_s}{R_{sh}} \quad (1)$$

doi: 10.1049/joe.2015.0125

$$I_{\rm pv} = (I_{\rm sc} + K_I(T - 298))\frac{G}{1000} \tag{2}$$

$$V_{\rm t} = \frac{ak_{\rm b}}{e}T \tag{3}$$

$$I_0 = I_{0,\rm ref}\left(\frac{T}{298}\right)^3 \exp\left(\frac{eE_g}{k_{\rm b}N_{\rm s}V_{\rm t}}\left(\frac{1}{298} - \frac{1}{T}\right)\right) \tag{4}$$

where $I_{\rm pv}$, I_0, $V_{\rm t}$, $N_{\rm s}$, $R_{\rm s}$, $R_{\rm sh}$, $I_{\rm sc}$, K_I, G, T and $k_{\rm b}$ are photo-generated current, dark-saturation current, thermal voltage, number of series cells a in PV panel, series resistance, shunt resistance, short-circuit current, short-circuit coefficient of temperature, solar radiation, temperature and Boltzmann's constant, respectively. $v_{\rm pv}$ and $i_{\rm pv}$ are output voltage and current, respectively, of the PV panel. $I_{0,\rm ref}$, e and E_g are reference dark-saturation current, charge of an electron and energy of a photon constant, respectively.

Figs. 1*b* and *c* show the converter for different switching operations. Here, u is the control signal of the boost converter which is a series of pulses with duty-ratio δ. Referring Fig. 1*b*, when the switch (Sw) is OFF, then

$$\begin{cases} i_L = C_1\dot{v}_{\rm pv} + \dfrac{v_{\rm pv}}{C_1 r_{\rm pv}} \Rightarrow \dot{v}_{\rm pv} = \dfrac{1}{C_1}i_{\rm L} - \dfrac{1}{C_1 r_{\rm pv}}v_{\rm pv} \\ v_{\rm pv} = L\dot{i}_{\rm L} + v_{\rm dc} \Rightarrow \dot{i}_{\rm L} = \dfrac{1}{L}v_{\rm pv} - \dfrac{1}{L}v_{\rm dc} \end{cases} \tag{5}$$

where $r_{\rm pv}$ is the dynamic resistance of PV panel and defined as

$$r_{\rm pv} = -\frac{\partial v_{\rm pv}}{\partial i_{\rm pv}} \tag{6}$$

When the switch (Sw) is ON (Fig. 1*c*), then

$$\begin{cases} i_L = C_1\dot{v}_{\rm pv} + \dfrac{v_{\rm pv}}{C_1 r_{\rm pv}} \quad \Rightarrow \quad \dot{v}_{\rm pv} = \dfrac{1}{C_1}i_{\rm L} - \dfrac{1}{C_1 r_{\rm pv}}v_{\rm pv} \\ v_{\rm pv} = L\dot{i}_{\rm L} \quad \Rightarrow \quad \dot{i}_{\rm L} = \dfrac{1}{L}v_{\rm pv} \end{cases} \tag{7}$$

Let δ be the duty-ratio of the control signal u for controlling the switch Sw, and then (5)–(7) can be rewritten as

$$\begin{aligned} \dot{i}_{\rm L} &= \frac{1}{L}v_{\rm pv} - \bar{\delta}\frac{1}{L}v_{\rm dc} \\ \dot{v}_{\rm pv} &= \frac{1}{C_1}i_{\rm L} - \frac{1}{C_1 r_{\rm pv}}v_{\rm pv} \end{aligned} \tag{8}$$

where $\bar{\delta} = 1 - \delta$. Considering $v_{\rm pv}$ and $i_{\rm L}$ as state variables, the dynamics of the boost converter can be written in state-space form as

$$\dot{X} = f(X) + g(X)\delta \tag{9}$$

where

$$\left.\begin{aligned} X &= \begin{bmatrix} i_{\rm L} & v_{\rm pv} \end{bmatrix}^{\rm T} \\ f(X) &= \begin{bmatrix} \dfrac{v_{\rm pv}}{L} - \dfrac{v_{\rm dc}}{L} & \dfrac{v_{\rm dc}}{L} \\ \dfrac{i_{\rm L}}{C_1} & -\dfrac{1}{C_1 r_{\rm pv}}v_{\rm pv} \end{bmatrix} \\ g(X) &= \begin{bmatrix} \dfrac{v_{\rm dc}}{L} & 0 \end{bmatrix}^{\rm T} \end{aligned}\right\} \tag{10}$$

The MPPT control problem of the PV system can be formulated as follows. For MPP tracking operation, it is intended to develop an MPPT algorithm for generating reference operating voltage ($V_{\rm ref}$). Then, a DC/DC boost converter is used to adjust the PV voltage close to that of $V_{\rm ref}$. A control circuit helps the boost converter in this task by supplying appropriate switching control signal to the boost converter.

3 Design of the proposed adaptive DISMC-MPPT

The proposed DISMC-MPPT (Fig. 2*a*) is designed as follows. It consists of an MPPT algorithm, a boost converter and the DISMC. The dynamics of DC/DC boost converter is described in (9). Considering the switching control signal u from the DISMC subsystem, the inductor current ($i_{\rm L}$) of boost converter and PV voltage ($v_{\rm pv}$) are adjusted such that maximum power can be extracted from the PV system and load voltage $v_{\rm dc}$ can be maintained at a fixed value $V_{\rm dc}$. A new MPPT algorithm as shown in Fig. 2*b* is used in this paper for calculating the reference voltage $V_{\rm ref}$.

The proposed DISMC is designed as follows. Usually in a DC/DC converter, the duty-ratio δ of the switching signal u is such that $0 \le \delta \le 1$. As discussed in Section 2, the proposed DISMC-MPPT has the PWM-based switching signal u; hence it has only two logic states 0 and 1. The general switching law for a DC/DC boost converter is as follows

$$u = \begin{cases} 1; & \text{when } S < 0 \\ 0; & \text{when } S > 0 \end{cases} \tag{11}$$

where S is the proposed sliding surface that is defined as

$$S = a_1e_1 + a_2e_2 + a_3e_3 + a_4e_4 \tag{12}$$

The terms a_1–a_4 represent the sliding coefficients. The terms e_1–e_4 are voltage and current error signals and are defined as follows

$$\left.\begin{aligned} e_1 &= i_{\rm ref} - i_{\rm L} \\ e_2 &= V_{\rm ref} - \beta v_{\rm pv} \\ e_3 &= \int \left(V_{\rm ref} - \beta v_{\rm pv}\right) {\rm d}t \\ e_4 &= \int \left[\int \left(V_{\rm ref} - \beta v_{\rm pv}\right) {\rm d}t\right] {\rm d}t \end{aligned}\right\} \tag{13}$$

$$i_{\rm ref} = m\left(V_{\rm ref} - \beta v_{\rm pv}\right) \tag{14}$$

where m is the voltage error constant. On differentiating the state variables of (13) leads to [19]

$$\left.\begin{aligned} \dot{e}_1 &= \frac{\rm d}{{\rm d}t}\left[i_{\rm ref} - i_{\rm L}\right] = \frac{m\beta}{C_1}i_{c1} - \frac{v_{\rm pv}}{L} + \frac{v_{\rm dc}}{L} - \frac{v_{\rm dc}}{L}u \\ \dot{e}_2 &= \frac{\rm d}{{\rm d}t}\left[V_{\rm ref} - \beta v_{\rm pv}\right] = \frac{\beta}{C_1}i_{c1} \\ \dot{e}_3 &= V_{\rm ref} - \beta v_{\rm pv} \\ \dot{e}_4 &= \int \left[V_{\rm ref} - \beta v_{\rm pv}\right] {\rm d}t \end{aligned}\right\} \tag{15}$$

Taking derivative of S gives

$$\dot{S} = a_1\dot{e}_1 + a_2\dot{e}_2 + a_3\dot{e}_3 + a_4\dot{e}_4 \tag{16}$$

The equivalent control signal ($u_{\rm eq}$) can be obtained by solving

$$\dot{S} = 0 \tag{17}$$

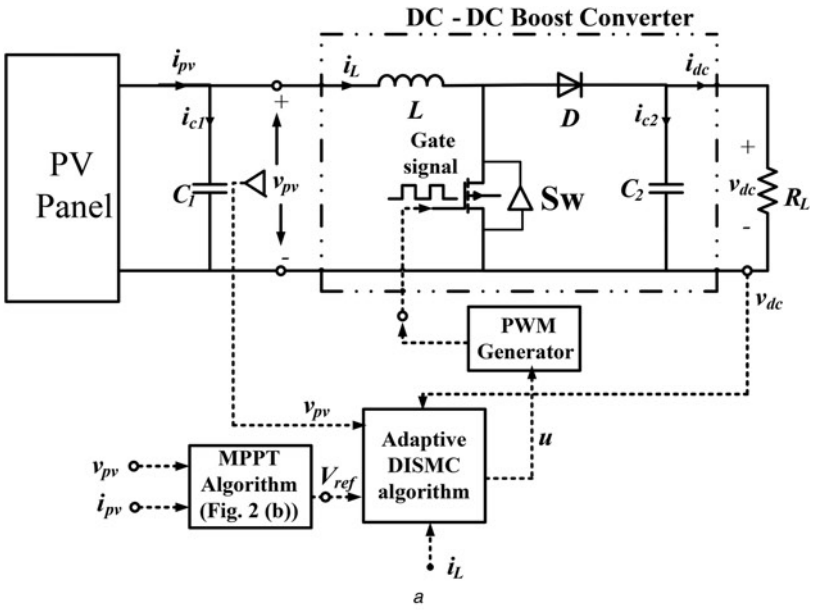

a

Step-1:	Input v_{pv} (k) and i_{pv} (k). V_{ref} (k) = v_{pv} (k)
Step-2:	Calculate $p_{pv}(k) = v_{pv}(k) \times i_{pv}(k)$
Step-3:	Calculate $dp_{pv}(k) = p_{pv}(k) - p_{pv}(k-1)$ and $dv_{pv}(k) = v_{pv}(k) - v_{pv}(k-1)$
Step-4:	Calculate $F(k) = \frac{dp_{pv}(k)}{dv_{pv}(k)}$
Step-5:	Calculate gradient of p_{pv} (k) as $g(k) = \frac{F(k) - F(k-1)}{v_{pv}(k) - v_{pv}(k-1)}$
Step-6:	If $F(k) > 0$ $\alpha = \varepsilon$, where α is the step-size and ε is a very small positive number Else if $F(k) < 0$ $\alpha = -\varepsilon$ Else if $F(k) = 0$ $\alpha = 0$
Step-7:	Update $V_{ref}(k+1) = V_{ref}(k) - \alpha g(k)$

b

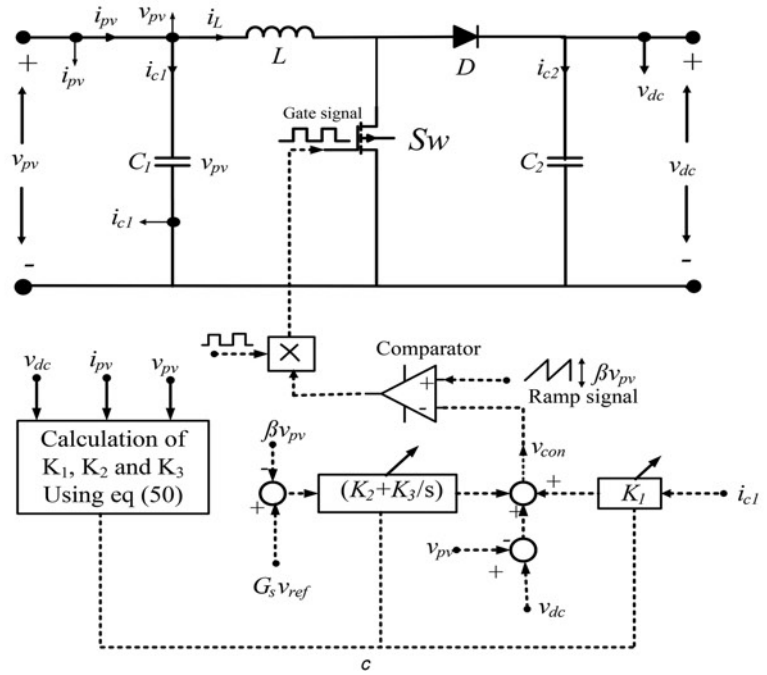

c

Fig. 2 *Design of the proposed adaptive DISMC-MPPT*
a Structure of the proposed adaptive DISMC-MPPT
b Proposed MPPT-algorithm for calculation of V_{ref}
c Controller circuit diagram of the proposed adaptive DISMC-MPPT

doi: 10.1049/joe.2015.0125

Applying (15) and (16) in (17) and then solving for δ_{eq} yields

$$\begin{aligned}\dot{S} &= a_1\dot{e}_1 + a_2\dot{e}_2 + a_3\dot{e}_3 + a_4\dot{e}_4 = 0\\ &\Rightarrow a_1\left(\frac{m\beta}{C_1}i_{c1} - \frac{v_{pv}}{L} + \frac{v_{dc}}{L} - \frac{v_{dc}}{L}\delta_{eq}\right) + a_2\left(\frac{\beta}{C_1}i_{c1}\right)\\ &\quad + a_3\left(V_{ref} - \beta v_{pv}\right) + a_4\int\left[V_{ref} - \beta v_{pv}\right]\mathrm{d}t = 0\end{aligned} \tag{18}$$

and

$$\begin{aligned}a_1\frac{v_{dc}}{L}\delta_{eq} &= a_1\left(\frac{m\beta}{C_1}i_{c1} - \frac{v_{pv}}{L} + \frac{v_{dc}}{L}\right) + a_2\left(\frac{\beta}{C_1}i_{c1}\right)\\ &\quad + a_3\left(V_{ref} - \beta v_{pv}\right) + a_4\int\left[V_{ref} - \beta v_{pv}\right]\mathrm{d}t\end{aligned} \tag{19}$$

Hence, equivalent duty-ratio of the control signal (δ_{eq}) is obtained as

$$\begin{aligned}\delta_{eq} &= \frac{\beta L}{v_{dc}C_1}\left(m + \frac{a_2}{a_1}\right)i_{c1} - \frac{v_{pv}}{v_{dc}} + 1 + \frac{a_3L}{v_{dc}a_1}\left(V_{ref} - \beta v_{pv}\right)\\ &\quad + \frac{a_4L}{v_{dc}a_1}\int\left[V_{ref} - \beta v_{pv}\right]\mathrm{d}t\end{aligned} \tag{20}$$

Let, v_{con} is the control voltage of DISMC-MPPT which can be calculated as

$$v_{con} = K_1 i_{c1} - v_{pv} + v_{dc} + K_2 e_2 + K_3 e_3 \tag{21}$$

where

$$\begin{aligned}v_{con} &= v_{dc}\delta_{eq}\\ K_1 &= \frac{\beta L}{C_1}\left(m + \frac{a_2}{a_1}\right)\\ K_2 &= \frac{a_3L}{a_1}\\ K_3 &= \frac{a_4L}{a_1}\end{aligned} \tag{22}$$

The DISMC-MPPT sliding surface parameters K_1, K_2 and K_3 are chosen such that existence and stability conditions would be satisfied. The circuit diagram of this DISMC-MPPT is shown in Fig. 2*c*. The functional responsibility of the proposed DISMC-MPPT is that for a given DC/DC boost converter with fixed values of capacitances C_1, C_2 and inductance L, it is required to find K_1, K_2 and K_3 such that the reaching and stability conditions are satisfied.

3.1 Reaching condition

Reaching condition is to be satisfied in order to ensure that the state trajectory of the system will be directed always toward the sliding surface from any initial conditions. To achieve this, the product of sliding function and its first derivative term must be negative according to Lyapunov's stability concept. Hence

$$\lim_{S\to 0} S\dot{S} < 0 \tag{23}$$

Referring (11) and (23), in a boost converter, if

$$u = 1 \Rightarrow \dot{S} > 0 \Rightarrow K_1 i_{c1} + K_2 e_2 + K_3 e_3 < v_{pv} \tag{24}$$

and when

$$u = 0 \Rightarrow \dot{S} < 0 \Rightarrow K_1 i_{c1} + K_2 e_2 + K_3 e_3 > \left(v_{pv} - v_{dc}\right) \tag{25}$$

At the steady state, (24) and (25) can be rewritten as follows

$$K_1 i_{c1(\min)} + K_2 e_{2(\max)} + K_3 e_{3(\max)} < v_{pv(ss)} \tag{26}$$

$$K_1 i_{c1(\max)} + K_2 e_{2(\min)} + K_3 e_{3(\min)} > \left(v_{pv(ss)} - v_{dc(\min)}\right) \tag{27}$$

where $v_{pv(ss)}$ is the PV panel voltage at steady state, $v_{dc(min)}$ is the minimum output voltage, $e_{22(min)}$ and $e_{22(max)}$ are minimum and maximum values of error e_2, respectively, $e_{23(min)}$ and $e_{23(max)}$ are minimum and maximum values of error e_{23}, respectively and $i_{c1(min)}$,$i_{c1(max)}$ are minimum and maximum inductor currents, respectively.

3.2 Stability condition

This condition ensures that the state trajectory remains in the sliding surface. The proposed adaptive DISMC-MPPT consists of both the current and voltage state variable terms in its structure. Hence, the sliding motion equation ($S = 0$) cannot be solved analytically. It can be solved by using the PV system and controller dynamics given by (9) and equivalent control signal given by (20) as follows. Substituting δ_{eq} from (20) into (9), we get

$$\left.\begin{aligned}\dot{i}_L &= -\frac{K_1}{L}i_{c1} + \frac{K_2}{L}\left(V_{ref} - \beta v_{pv}\right) + \frac{K_3}{L}\int\left(V_{ref} - \beta v_{pv}\right)\mathrm{d}t\\ \dot{v}_{pv} &= \frac{1}{C_1}i_L - \frac{1}{C_1 r_{pv}}v_{pv}\end{aligned}\right\} \tag{28}$$

$$\left.\begin{aligned}\Rightarrow \dot{i}_L &= -\frac{K_1}{L}\left(\frac{v_{pv}}{r_{pv}} - i_L\right) + \frac{K_2}{L}\left(V_{ref} - \beta v_{pv}\right) + \frac{K_3}{L}\int\left(V_{ref} - \beta v_{pv}\right)\mathrm{d}t\\ \dot{v}_{pv} &= \frac{1}{C_1}i_L - \frac{1}{C_1 r_{pv}}v_{pv}\end{aligned}\right\} \tag{29}$$

$$\left.\begin{aligned}\Rightarrow \dot{i}_L &= \frac{K_1}{L}i_L - \frac{K_1}{Lr_{pv}}v_{pv} + \frac{K_2}{L}\left(V_{ref} - \beta v_{pv}\right) + \frac{K_3}{L}\int\left(V_{ref} - \beta v_{pv}\right)\mathrm{d}t\\ \dot{v}_{pv} &= \frac{1}{C_1}i_L - \frac{1}{C_1 r_{pv}}v_{pv}\end{aligned}\right\} \tag{30}$$

Equation (30) can be rewritten as

$$\left.\begin{aligned}\dot{\tilde{i}}_L &= \beta_{11}\tilde{i}_L + \beta_{12}\tilde{v}_{pv} + \beta_{13}\int\tilde{v}_{pv}\,\mathrm{d}t\\ \dot{\tilde{v}}_{pv} &= \beta_{21}\tilde{i}_L + \beta_{22}\tilde{v}_{pv} + \beta_{23}\int\tilde{v}_{pv}\,\mathrm{d}t\\ \frac{\mathrm{d}}{\mathrm{d}t}\left(\int\tilde{v}_{pv}\,\mathrm{d}t\right) &= \beta_{31}\tilde{i}_L + \beta_{32}\tilde{v}_{pv} + \beta_{33}\int\tilde{v}_{pv}\,\mathrm{d}t\end{aligned}\right\} \tag{31}$$

where

$$\left.\begin{aligned}&\tilde{i}_L = i_L \quad \tilde{v}_{pv} = V_{ref} - \beta v_{pv}\\ &\beta_{11} = \frac{K_1}{L} \quad \beta_{12} = -\left(\frac{K_1}{r_{pv}L} + \frac{K_2}{L}\right) \quad \beta_{13} = \frac{K_1}{L}\\ &\beta_{21} = \frac{1}{C_1} \quad \beta_{22} = -\frac{1}{C_1 r_{pv}} \quad \beta_{23} = 0\\ &\beta_{31} = 0 \quad \beta_{32} = 1 \quad \beta_{33} = 0\end{aligned}\right\} \tag{32}$$

Characteristic equation of the linearised PV system becomes

$$\begin{vmatrix} s-\beta_{11} & -\beta_{12} & -\beta_{13} \\ -\beta_{21} & s-\beta_{22} & -\beta_{23} \\ -\beta_{31} & -\beta_{32} & s-\beta_{33} \end{vmatrix} = 0 \Rightarrow s^3+\beta_1 s^2+\beta_2 s+\beta_3 = 0 \tag{33}$$

where

$$\begin{cases} \beta_1 = -(\beta_{11}+\beta_{22}) \\ \beta_2 = -\beta_{23}+\beta_{11}\beta_{22}-\beta_{12}\beta_{21} \\ \beta_3 = \beta_{11}\beta_{23}-\beta_{13}\beta_{21} \end{cases} \tag{34}$$

Characteristic (33) can be used to apply Routh–Hurwitz criterion for determining stability condition as follows

$$\begin{bmatrix} s^3 & 1 & \beta_2 \\ s^2 & \beta_1 & \beta_3 \\ s^1 & \dfrac{\beta_3-\beta_1\beta_2}{\beta_1} & 0 \\ s^0 & \beta_3 & 0 \end{bmatrix} \tag{35}$$

From (35), at critically stable conditions

$$\frac{\beta_3-\beta_1\beta_2}{\beta_1} = 0 \tag{36}$$

The above conditions such as reaching and stability conditions should be satisfied to ensure the closed-loop stability of the PV system. Thus, K_1, K_2 and K_3 should be chosen such that (26), (27) and (36) are valid.

3.3 Adaptive tuning of DISMC parameters K_1, K_2 and K_3

A second-order stable system with un-damped natural frequency ω_n and damping-ratio ζ is usually in the form of

$$\frac{\mathrm{d}^2x}{\mathrm{d}t^2}+2\zeta\omega_n\frac{\mathrm{d}x}{\mathrm{d}t}+\omega_n^2 = 0 \tag{37}$$

Laplace transform of (40) is

$$\left(s^2+2\zeta\omega_n s+\omega_n^2\right)X(s) = 0 \Rightarrow s^2+2\zeta\omega_n s+\omega_n^2 = 0 \tag{38}$$

The PV system is also a second-order system with

$$\omega_n = \frac{v_{\mathrm{pv}}}{v_{\mathrm{dc}}}\sqrt{\frac{1}{LC_1}}$$

In this PV system, in critically stable condition v_{pv} will be equal to V_{ref} at steady state if

$$i_{\mathrm{ref}}-i_{\mathrm{L}} = 0 \Rightarrow e_1 = 0 \tag{39}$$

At steady state, the following condition is also satisfied

$$S = 0 \Rightarrow a_1e_1+a_2e_2+a_3e_3+a_4e_4 = 0 \tag{40}$$

Applying (39) in (40), one would get

$$\begin{aligned} a_2e_2+a_3e_3+a_4e_4 &= 0 \\ \Rightarrow a_2e_2+a_3\int e_2\,\mathrm{d}t+a_4\iint e_2\,\mathrm{d}t\,\mathrm{d}t &= 0 \end{aligned} \tag{41}$$

Applying Laplace transform, (41) can be rewritten as

$$\begin{aligned} a_2E_2(s)+\frac{a_3}{s}E_2(s)+\frac{a_4}{s^2}E_2(s) &= 0 \\ \Rightarrow s^2+\frac{a_3}{a_2}s+\frac{a_4}{a_2} &= 0 \end{aligned} \tag{42}$$

Comparing (38) with (42), the following relationships can be derived:

$$2\zeta\omega_n = \frac{a_3}{a_2}, \quad \omega_n^2 = \frac{a_4}{a_2} \tag{43}$$

or

$$\frac{a_3}{a_2} = 2\zeta\frac{1}{\sqrt{LC_1}}, \quad \frac{a_4}{a_2} = LC_1 \tag{44}$$

Comparing (22), (43) and (44), one would get the following:

$$\begin{aligned} &\frac{K_2}{K_3} = \frac{a_3}{a_4} = \frac{2\zeta}{\omega_n} \\ &a_1 = \frac{a_3L}{K_2} \Rightarrow K_1 = \frac{\beta L}{C_1}\left(m+\frac{a_2}{a_3L}K_2\right) \end{aligned} \tag{45}$$

Let t_{s} be the settling time of the PV system with DISMC. It can be described as

$$t_{\mathrm{s}} = \frac{4}{\zeta\omega_n} \Rightarrow \zeta\omega_n = \frac{4}{t_{\mathrm{s}}} \tag{46}$$

Then, (45) can be rewritten as

$$\begin{aligned} \frac{K_2}{K_3} = \frac{8}{t_{\mathrm{s}}\omega_n^2} &= \frac{8\times LC_1}{t_{\mathrm{s}}}\left(\frac{v_{\mathrm{dc}}}{v_{\mathrm{pv}}}\right)^2 \\ \Rightarrow K_3 &= \left(\frac{t_{\mathrm{s}}}{8\times LC_1}\right)\left(\frac{v_{\mathrm{pv}}}{v_{\mathrm{dc}}}\right)^2K_2 \end{aligned} \tag{47}$$

Table 1 Values of components of the proposed DISMC-MPPT

PV panel		Prototype PV system	
Components	Value	Components	Value
I_{sc}, A	2.8	R_{L}, Ω	100
V_{oc}, V	21.6	L, mH	5
I_{mpp}, A	2.2	C_1, μF	380
V_{mpp}, V	18.2	C_2, μF	330
K_V, %/°K	−0.76	switching frequency (f_{s}), kHz	10
K_I, %/°K	0.06	β, m	0.8, 10
series cells per module N_{s}	36	v_{pv}, V	0–113
number of PV modules	5	r_{pv}, Ω	0–10

Using (46) and (47) in (48), one can get

$$K_1 = \frac{\beta L}{C_1}\left(m + \frac{t_s}{8L}K_2\right) \tag{48}$$

Again referring (36), the following relationship is valid for critically stable condition:

$$K_2 = \frac{K_3 L}{K_1 - (L/C_1 r_{pv})} \Rightarrow K_3 = \frac{K_2}{L}\left(K_1 - \frac{L}{C_1 r_{pv}}\right) \tag{49}$$

Solving (47), (48) and (49), K_1, K_2 and K_3 can be determined as follows:

$$\left.\begin{aligned} K_1 &= \frac{t_s}{8C_1}\left(\frac{v_{pv}}{v_{dc}}\right)^2 + \frac{L}{C_1 r_{pv}} \\ K_2 &= \frac{8}{\beta t_s}\left(\frac{t_s}{8}\left(\frac{v_{pv}}{v_{dc}}\right)^2 + \frac{L}{C_1 r_{pv}} - m\beta L\right) \\ K_3 &= \frac{K_2}{L}\left(K_1 - \frac{L}{C_1 r_{pv}}\right) \end{aligned}\right\} \tag{50}$$

In (50), L and C_1 are fixed. The values of m, β and t_s can be chosen by the designer. However, the value of r_{pv} is dependent on weather condition hence r_{pv} changes with every variation in weather conditions. Since K_1, K_2 and K_3 are functions of r_{pv}, their values also adopted with r_{pv} using (6). Owing to PWM control action in the DISMC-MPPT, there is a high-frequency switching operation.

This switching operation causes high-frequency chattering in the output. The chattering magnitude (h) in PV voltage output signal (v_{pv}) is calculated as follows

$$h = h_1 - h_2 \tag{51}$$

where h_1 and h_2 are the upper and lower bounds of the chattering in v_{pv}. Similarly, the steady-state error (SSE) of v_{pv} during tracking operation can be calculated as

$$\text{SSE} = V_{ref} - \left[h_2 + \frac{(h_1 - h_2)}{2}\right] \tag{52}$$

where V_{ref} is the reference PV voltage at which the operating point of the PV system lies at MPP. The objective of the proposed DISMC is to minimise the SSE with low chattering magnitude. Efficiency of an MPPT can be evaluated as follows

$$\eta_{MPPT}(\%) = \left|\frac{P_{mpp(calculated)} - P_{mpp(measured)}}{P_{mpp(calculated)}}\right| \times 100 \tag{53}$$

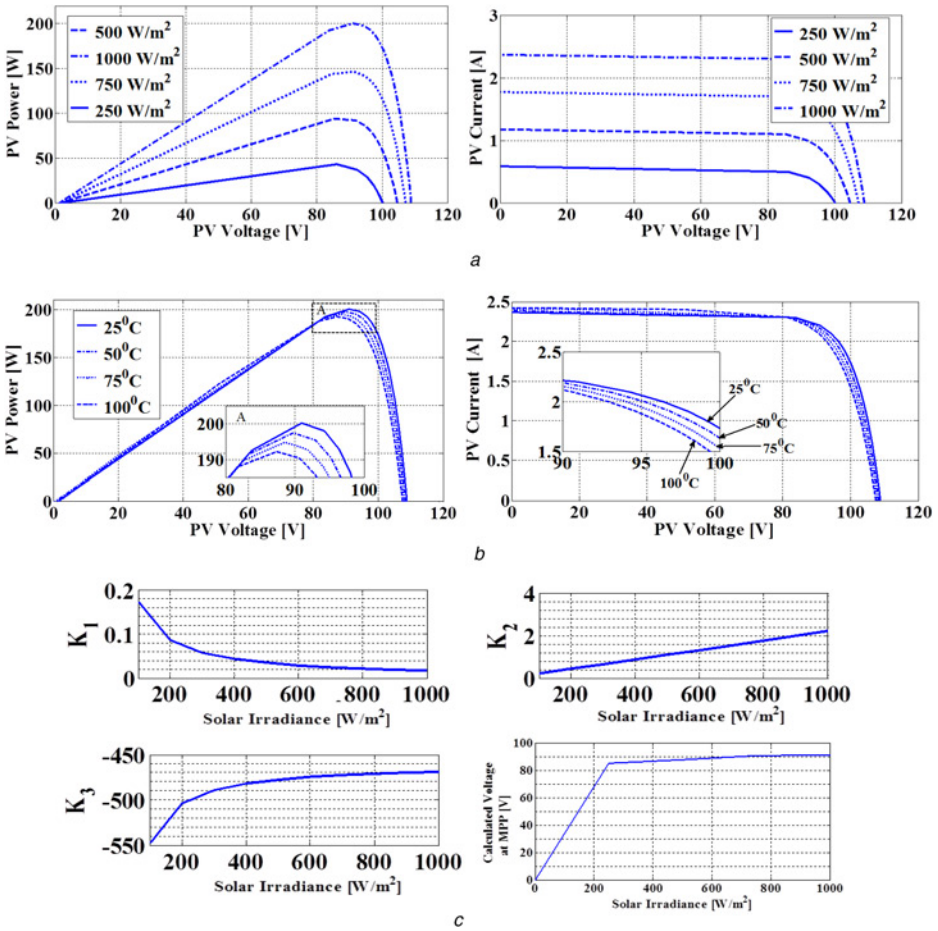

Fig. 3 *Simulation results*
a P–V characteristics and I–V characteristics of studied PV panel at different solar irradiances
b P–V characteristics and I–V characteristics at different solar irradiances
c Values of K_1, K_2, K_3 and V_{ref} of the tested PV system with DISMC-MPPT for variations in G from 100 to 1000 W/m^2

doi: 10.1049/joe.2015.0125

Table 2 Value of V_{ref} of the studied PV panel calculated at different solar radiations

	At different temperature			
	25	50	75	100
V_{oc}, V	108.9	108.4	108	107.5
V_{ref}, V	92	89.8	88.5	87.5
P_{max}, W	200	197.5	195	192.5
	At different solar radiation			
	250	500	750	1000
V_{oc}, V	101	104.5	107	109
V_{ref}, V	86	88.5	91	92
P_{max}, W	43	94	146	200

4 Results and discussion

4.1 Simulation results

The MPPT tracking performance of the proposed adaptive DISMC-MPPT was verified on a 0.2 kW PV system whose parameters are shown in Table 1. This PV system consists of which has five 40 W PV modules. *I–V* and *P–V* characteristics of the studied PV panel are shown in Figs. 3*a* and *b*. These simulated tracking performances are evaluated and tested using MATLAB/Simulink.

In this paper, calculated PV panel voltage at MPP of the studied PV system has been considered as V_{ref} while designing the proposed adaptive DISMC-MPPT controller. This V_{ref} is calculated online for every change in solar irradiance or temperature using the MPPT algorithm shown in Fig. 2*a*. The values of V_{ref} for the studied PV system at different solar irradiance or temperature are shown in Table 2.

For efficient tracking of the V_{ref} of the studied PV panel, the parameters of the values of different components are used in this paper as shown in Table 1. In this table, the values of the components of the given DC/DC boost converter, that is: inductor (L) and capacitors (C_1 and C_2) are constant. Taking these values of L, C_1 and C_2, the parameters K_1, K_2 and K_3 were calculated using (50). These parameters K_1, K_2 and K_3 are updated along with V_{ref} for every variation in weather changes as shown in Fig. 3*c*.

Furthermore, to test the efficacy of the proposed adaptive DISMC-MPPT, its performances are compared with that of two existing DISMC-MPPTs with different sliding surfaces such as Jiao's sliding surface [20] and Tan's sliding surface [22]. Fig. 4 shows the chattering and SSE of the studied PV system with the proposed adaptive DISMC-MPPT with that of DISMC-MPPT [20], DISMC-MPPT [22] and P&O MPPT [6] and adaptive P&O MPPT [8] at 250 W/m^2 and 25°C. In these figures, h_1 and h_2 are

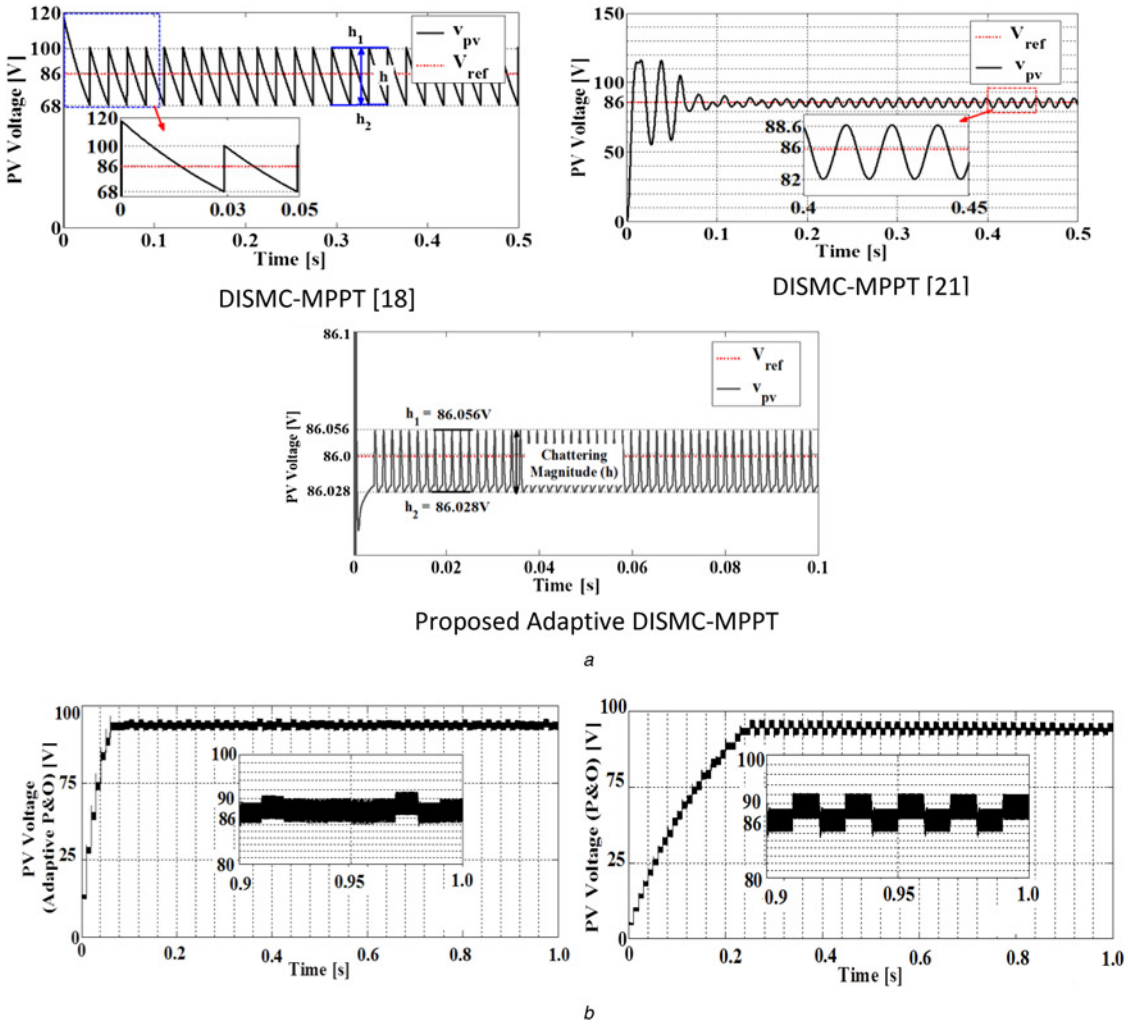

Fig. 4 *Comparison of chattering in studied PV system output voltage signal at 500 W/m^2 and 25°C*
a DISMC-MPPT [20], DISMC-MPPT [23], the proposed adaptive DISMC-MPPT controller, adaptive P&O MPPT [8]
b P&O MPPT [6]

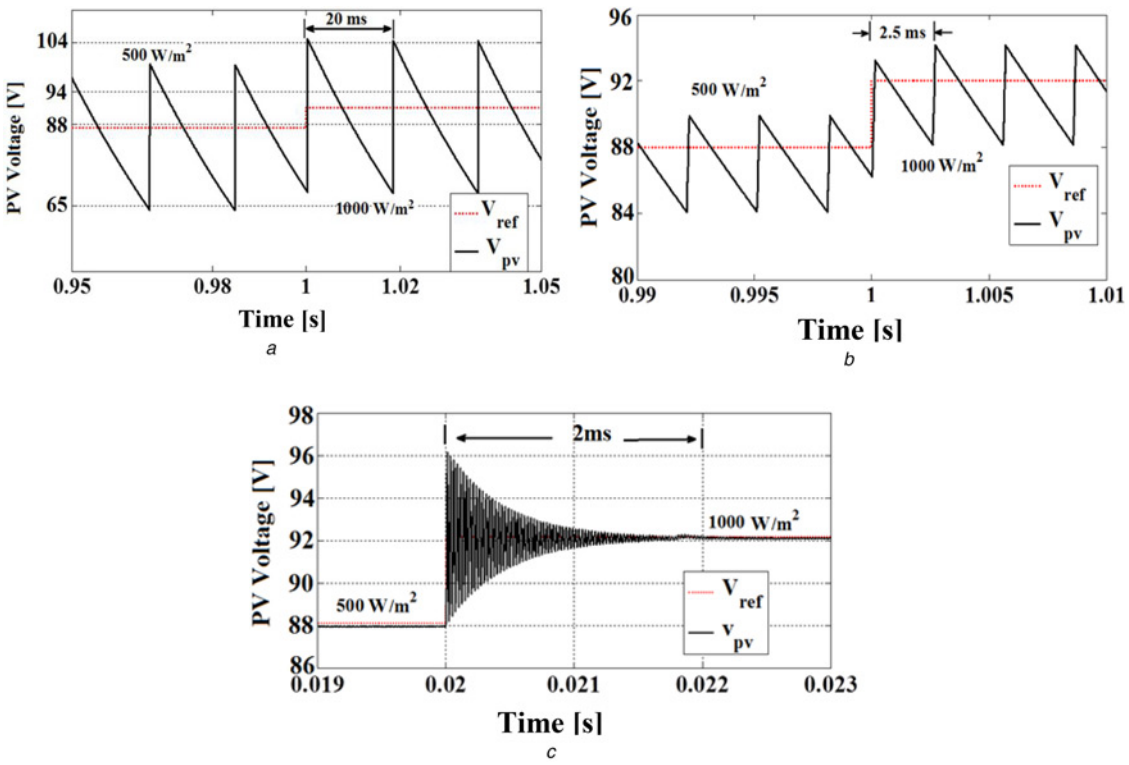

Fig. 5 *Comparison of MPP tracking behaviour of PV system with*
a DISMC-MPPT [20]
b DISMC-MPPT [21]
c the proposed DISMC-MPPT for step-change in solar irradiation from 500 to 1000 W/m^2

the highest and lowest chattering points, respectively, of the PV voltage at steady state of the tracking operation.

In Fig. 4, it can be seen that the PV voltage with DISMC-MPPT [20] is fluctuating between 100 and 68 V. Maximum overshoot and tracking time in this case is 120 V − 86 V = 34 V and 30 ms, respectively. It is also found that although the PV voltage with DISMC-MPPT [20] is fluctuating less than that of DISMC-MPPT [23] such as between 88.6 and 82 V, but its tracking time is 200 ms. Moreover, maximum overshoot of PV voltage in this case is almost same as that of DISMC-MPPT [20]. In case of the proposed DISMC, maximum overshoot and tracking time is 86.1 V − 86.0 V = 0.1 V and 5 ms, respectively. The PV voltage oscillates between 86.056 and 86.028 V, hence voltage fluctuation in this case is less than that of both DISMC-MPPT [20] and DISMC-MPPT [23]. It can also be seen that tracking time for P&O MPPT and adaptive P&O MPPT are 0.15 and 0.3 s, respectively. PV voltage fluctuation during MPP tracking in case of adaptive P&O MPPT is between 86 and 90 V, whereas in case of P&O MPPT is between 84 and 92 V. Hence the chattering magnitude h for P&O MPPT and adaptive P&O MPPT are calculated using equation (54) as 4 and 8 V, respectively. Therefore, it can be seen that both tracking time and PV voltage fluctuation are lesser in case of the proposed adaptive DISMC-MPPT than that of P&O MPPT and adaptive P&O MPPT.

Figs. 5*a–c* show the behaviour of the PV voltage during step-change in solar radiation from 500 to 1000 W/m^2. Referring these figures, it is found that tracking time in case of the proposed adaptive DISMC-MPPT, DISMC-MPPT [20] and DISMC-MPPT [23] are 2, 20, and 2.5 ms, respectively. Furthermore, the proposed DISMC-MPPT performs efficiently with less maximum over-shoot and chattering. Therefore, tracking response in case of the proposed adaptive DISMC-MPPT is better than that of DISMC-MPPT [20] and DISMC-MPPT [23].

Controller properties of P&O MPPT [6], adaptive P&O MPPT [8], DIMC-MPPT [20], DIMC-MPPT [23] and the proposed adaptive DIMC-MPPT and their tracking behaviours are summarised in Table 3. In this table, the chattering magnitude (h) and SSE have been calculated using equations (54) and (55), respectively. It can be seen from this table that the proposed adaptive DISMC-MPPT has less SSE (2 mV) and less h (2.8 mV) than that of P&O MPPT [6], adaptive P&O MPPT [8], DISMC-MPPT [20] and DIMC-MPPT [23].

Table 3 Comparative study of simulated results of MPPT controller properties and tracking responses in case of the proposed adaptive DISMC-MPPT with that of P&O MPPT [6], adaptive P&O MPPT [8], DISMC-MPPT [20] and DISMC-MPPT [21]

Controller properties	P&O [6]	Adaptive P&O [8]	DISMC-MPPT [20]	DISMC-MPPT [21]	Proposed adaptive DISMC-MPPT
controlling action	fixed	adaptive	fixed	fixed	adaptive
complexity	less	less	less	more	less
tracking time	0.3 s	0.15 s	22 ms	25 ms	5 ms
chattering	8 V	4 V	32 V	4.6 V	28 mV
SSE	0.5 V	0.5 V	8 V	1.7 V	14 mV
settling time during step-change in input, ms	2.5	20	2.5	20	2

4.2 *Experimental results*

The prototype of the PV system is developed for stand-alone application. It consists of PV arrays, DC/DC boost converter, inverter, SPARTAN 3A FPGA board, signal conditioners (voltage and current sensors), personal computer and analogue filtering circuits as shown in Fig. 6*a*. Fig. 6*b* shows the PV array where five PV panels are connected in series.

P–V characteristics of the prototype PV system at two practical weather conditions such as case I (916 W/m^2) and case II (958 W/m^2) are shown in Fig. 6*c*. It can be seen from this figure that open-circuit voltages of PV panel at case I and case II are 108 and 109 V, respectively.

Fig. 7 shows different experimental results obtained from experiments performed on the prototype PV system. The first figure of Fig. 7*a* shows the PV voltage at constant weather condition of case I. This PV voltage can be seen as same as the open-circuit voltage of the PV panel (108 V). The tracking behaviours of PV system with P&O [6], adaptive P&O [8] and DISMC-MPPT [23] are shown in second, third and fourth figures of Fig. 7*a*, respectively. Fig. 7*b* shows the MPP tracking of PV system with the proposed adaptive DISMC-MPPT. In all these figures of Figs. 7*a* and *b*, 'A' denotes the open-circuit condition when MPPT is OFF, 'B' denotes MPP tracking period and 'C' denotes steady-state MPPT operation. It is found that tracking periods are 1.6, 1.5, 1.4 and 1 s in case of P&O [6], adaptive P&O [8], DISMC-MPPT [16] and the proposed adaptive DISMC-MPPT, respectively. Similarly, voltage fluctuations during MPPT operation at steady state can be seen as 8, 5, 4 and 2 V for P&O [6], adaptive P&O [8], DISMC-MPPT [22] and the proposed adaptive DISMC-MPPT, respectively. Therefore, it is experimentally also proved that the proposed adaptive DISMC-MPPT possesses better tracking behaviour than P&O [6], adaptive P&O [8], DISMC-MPPT [22] and the proposed adaptive DISMC-MPPT. The experimental results showing variation in PV voltage and current for variation in weather condition are shown in Fig. 7*c*. In this figure, it can be seen that when PV voltage varies from 52 to 46 V, the PV current also rises from 1.19 to 1.24 A. The corresponding powers are calculated to be 61.9 and 57 W.

Figs. 8*a–d* show different experimental results obtained from the prototype PV system with the proposed adaptive DISMC-MPPT during MPP tracking operation at 248 W/m^2 and 32°C. PV voltage at this condition is obtained as 82.4 V as shown in Fig. 8*a*. Fig. 8*a* also shows that duty-ratio of gate pulse of converter is 52.4%. It is shown in Fig. 8*b* that the DC-link voltage is 173.2 V.

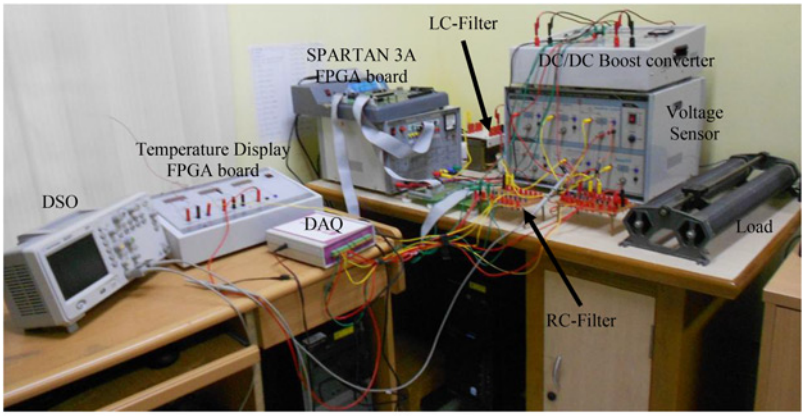

a

b

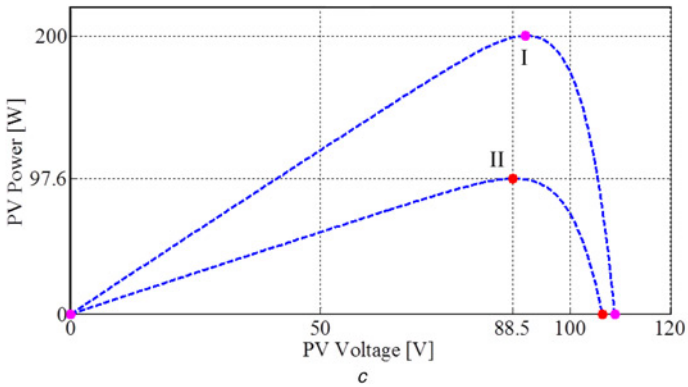

c

Fig. 6 *Experimental results*
a 0.2 kW prototype PV system
b PV array
c *P–V* characteristics of the PV system at case I (916 W/m^2) and case II (958 W/m^2)

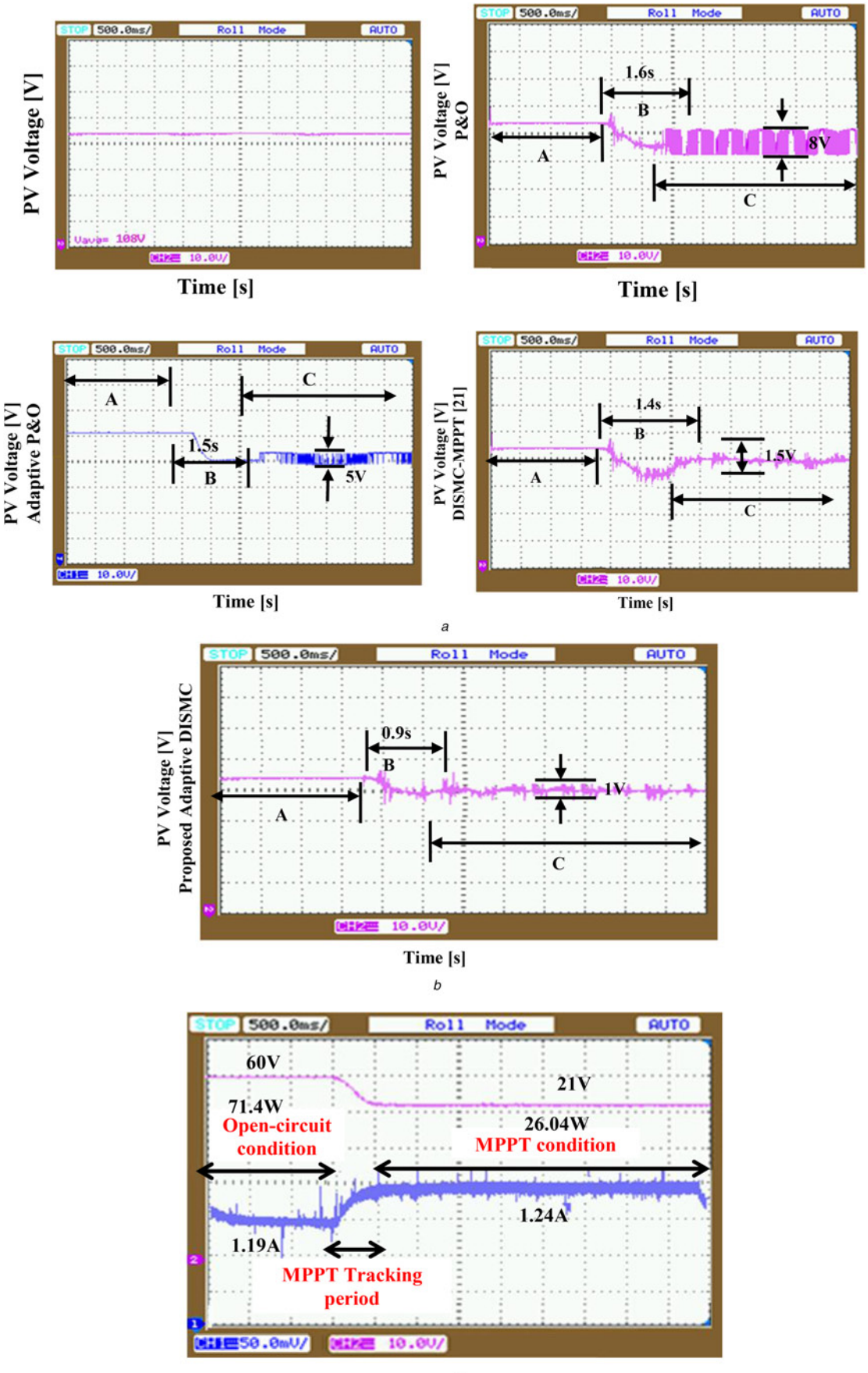

Fig. 7 *Experimental results of prototype PV system*
a PV voltage without MPPT operation at constant solar irradiance, PV voltage with P&O MPPT [6], adaptive P&O MPPT [8], DISMC-MPPT [23]
b PV voltage with adaptive DISMC-MPPT
c PV voltage and PV current with variation in solar irradiance with adaptive DISMC-MPPT (scales: *x*-axis 0.5 s/div and *y*-axis 10 V/div)

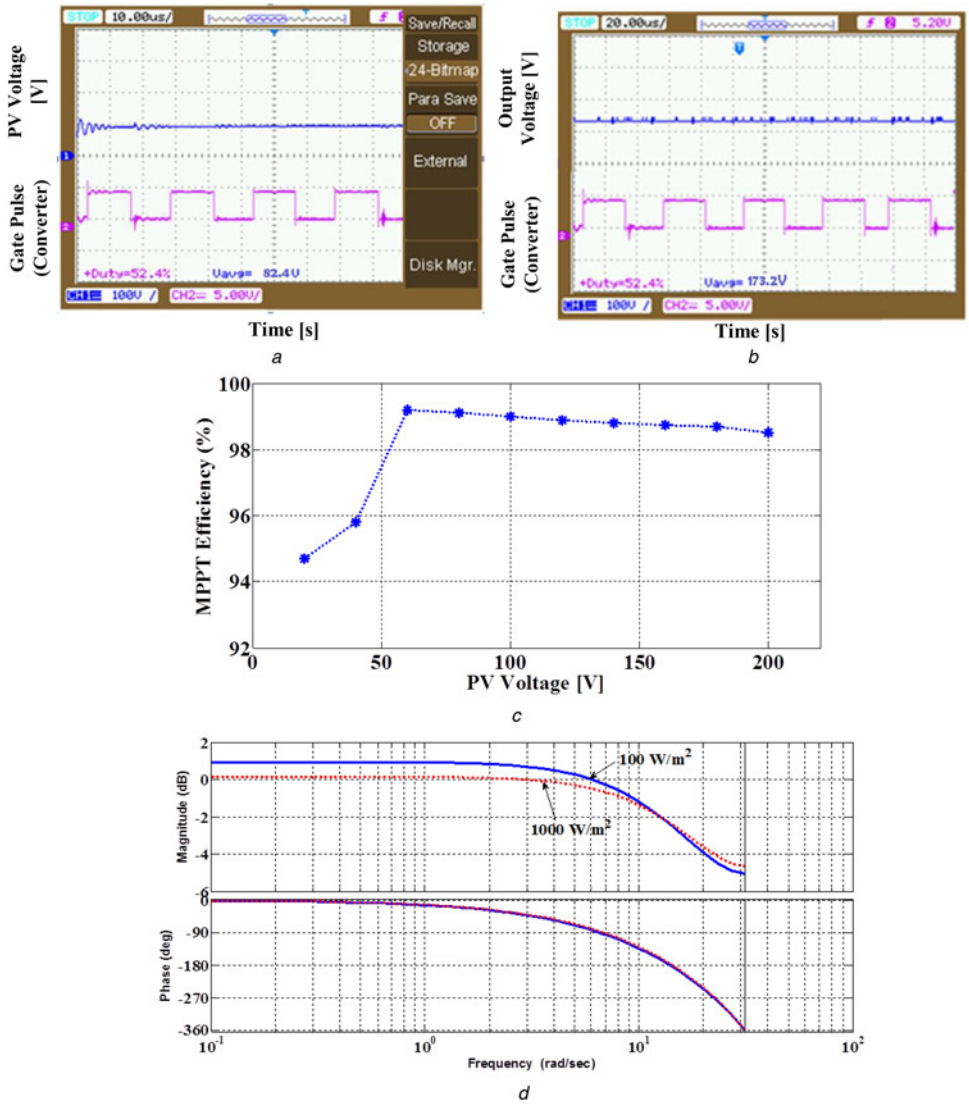

Fig. 8 *Experimental results of prototype PV system at*
a PV voltage and converter gate pulse
b PV voltage and converter gate pulse for solar irradiance of 248 W/m^2
c MPP tracking efficiency of PV system with proposed adaptive DISMC-MPPT at different PV power output
d Stability in case of the proposed adaptive DISMC-MPPT at different solar irradiances

For the validity of introducing a new MPPT, it is very important to check MPPT efficiency of the studied PV system using this MPPT. Fig. 8*c* shows the MPPT efficiency (53) of the PV system with the proposed adaptive DISMC-MPPT at different PV power outputs. It can be seen that the MPPT efficiency of the studied PV system is more than 90% in almost all power range of the PV system. Further referring [25], overall efficiency of the PV system (MPPT+inverter+load) with the proposed adaptive DISMC-MPPT is calculated to be 88.6% (maximum) and 79.5% (minimum).

In Fig. 8*d*, bode plot of the studied PV system with the proposed adaptive DISMC-MPPT is shown. In this figure, it is clearly seen that the PV system is stable both for 1000 and 100 W/m^2. Therefore, the PV system with the proposed adaptive DISMC-MPPT maintains its stability for a wide range of solar irradiance.

5 Conclusions

This paper proposed an adaptive DISMC-MPPT with a new double-integral-sliding surface for tracking MPPs of a PV system. The PWM mechanism of this adaptive DISMC-MPPT adds advantages such as simple control structure and fixed frequency operation. Furthermore, the selection of the SMC coefficients taking account the reaching and stability conditions facilitates with fast response and guaranteed stability. The efficacy of the proposed adaptive DISMC-MPPT was verified comparing with P&O MPPT [6], adaptive P&O MPPT [8], and three DISMC-MPPTs such as DISMC-MPPT [18], DISMC-MPPT [20] and DISMC-MPPT [21] that are with different sliding surfaces. From the comparison, it is found that with less number of components and control variables than DISMC-MPPT [18], the proposed adaptive DISMC-MPPT needs less tracking time and possesses less chattering than that of P&O MPPT [6], adaptive P&O MPPT [8], DISMC-MPPT [18], DISMC-MPPT [20] and DISMC-MPPT [21]. Hence, the proposed adaptive DISMC-MPPT is found to be an efficient MPP tracking of PV system perfectly balancing the control structure complexity, chattering in output signal and response time.

6 References

[1] Esram T., Chapman P.L.: 'Comparison of photovoltaic array maximum power point tracking techniques', *IEEE Trans. Energy Convers.*, 2007, **22**, (2), pp. 439–449

[2] Subudhi B., Pradhan R.: 'A comparative study of maximum power point tracking techniques for photovoltaic system', *IEEE Trans. Sust. Energy*, 2013, **4**, (1), pp. 89–98
[3] Liu F., Kang Y., Zhang Y., Duan S.: 'Comparison of P&O and hill climbing MPPT methods for grid-connected PV converter'. Third IEEE Conf. on Industrial Electronics and Applications (ICIEA), 2008, pp. 804–807
[4] Sokolov M., Shmilovitz D.: 'A modified MPPT scheme for accelerated convergence', *IEEE Trans. Energy Convers.*, 2008, **23**, (4), pp. 1105–1107
[5] Dounis A.I., Kofinas P., Alafodimos C., Tseles D.: 'Adaptive fuzzy gain scheduling PID controller for maximum power point tracking of photovoltaic system', *Renew. Energy*, 2013, **60**, (1), pp. 202–214
[6] Safari A., Mekhilef S.: 'Simulation and hardware implementation of incremental conductance MPPT with direct control method using Cuk converter', *IEEE Trans. Ind. Electron.*, 2011, **58**, (4), pp. 1154–1161
[7] Abdelsalam A.K., Massoud A.M., Ahmed S., Enjeti P.N.: 'High- performance adaptive perturb and observe MPPT technique for photovoltaic-based micro grids', *IEEE Trans. Power Electron. Convers.*, 2011, **26**, (4), pp. 1010–1021
[8] Liu F., Duan S., Liu F., Liu B., Kang Y.: 'A variable step size INC MPPT method for PV systems', *IEEE Trans. Ind. Electron.*, 2008, **55**, (7), pp. 2622–2628
[9] Petreus D., Pătărău T., Dărăban S., Morel C., Morley B.: 'A novel maximum power point tracker based on analog and digital control loops', *Sol. Energy*, 2011, **85**, (1), pp. 588–600
[10] Moura S.J., Chang Y.A.: 'Lyapunov-based switched extremum seeking for photovoltaic power maximization', *Control Eng. Pract.*, 2013, **21**, (1), pp. 971–980
[11] Chu C., Chen C.: 'Robust maximum power point tracking method for photovoltaic cells A sliding mode control approach', *Sol. Energy*, 2009, **8**, (1), pp. 1370–1378
[12] Chan C.Y.: 'A nonlinear control for DC-DC converters', *IEEE Trans. Power Electron.*, 2007, **22**, (1), pp. 216–222
[13] Bianconi E., Calvente J., Giral R., *ET AL.*: 'A fast current-based MPPT technique employing sliding mode control', *IEEE Trans. Ind. Electron.*, 2013, **60**, (3), pp. 1168–1178
[14] Levron Y., Shmilovitz D.: 'Maximum power point tracking employing sliding-mode control', *IEEE Trans. Circuits Syst. (I)*, 2013, **60**, (3), pp. 724–731
[15] Pastor A., Salamero L., Aroudi A., *ET AL.*: 'Synthesis of loss-free resistors based on sliding-mode control and its applications in power processing', *Control Eng. Pract.*, 2013, **21**, (1), pp. 689–699
[16] Alqahtani A., Utkin V.: 'Self-optimization of photovoltaic system power generation based on sliding mode control'. Proc. of IECON'12, 2012
[17] Fei J., Hou S.: 'Adaptive fuzzy control with fuzzy sliding switching for active power filter', *Trans. Inst. Meas. Control*, 2013, **35**, (8), pp. 1094–1103
[18] Ma K., Fei J.: 'Model reference adaptive fuzzy control of a shunt active power filter', *J. Intell. Fuzzy Control*, 2015, **28**, (1), pp. 485–494
[19] Tan S., Lai Y., Tse C., Salamero L., Wu C.: 'A fast-response sliding mode controller for boost-type converters with a wide range of operating conditions', *IEEE Trans. Ind. Electron.*, 2007, **54**, (6), pp. 3276–3286
[20] Tan S., Lai Y., Tse C.: 'Indirect sliding mode control of power converters via double integral sliding surface', *IEEE Trans. Power Electron.*, 2008, **23**, (2), pp. 600–610
[21] Jiao Y., Luo F.L.: 'An improved sliding mode controller for boost converter in solar energy system'. Fourth IEEE Congress on Industrial Electronics and Applications (ICIEA 2009), China, 2009
[22] Jiao Y., Luo F.L., Zhu M.: 'Generalized modeling and sliding mode control for n-cell cascade super-lift DC-DC converters', *IET Power Electron.*, 2010, **4**, (5), pp. 532–540
[23] Pradhan R., Subudhi B.: 'A new digital double integral sliding mode maximum power point tracker for photovoltaic power generation application'. Ninth IEEE ICSET, Nepal, 2012
[24] Subudhi B., Pradhan R.: 'A comparative study on PV panel parameter extraction methods', *Int. J. Renew. Energy Technol. (Inderscience)*, 2012, **3**, (3), pp. 295–315
[25] López-Santos O., López-Santos O., Martínez-Salamero L., *ET AL.*: 'Efficiency analysis of a sliding-mode controlled quadratic boost converter', *IET Power Electron.*, 2013, **6**, (2), pp. 364–373